Mechanics of Composite Materials, Vol. 46, No. 3, 2010

NUMERICAL ANALYSIS OF THE EFFECT OF MEMBRANE PRELOADS ON THE LOW-SPEED IMPACT RESPONSE OF COMPOSITE LAMINATES

D. Ghelli and G. Minak*

Keywords*: laminates, impact, membrane preload, finite-element analysis*

This article presents a comprehensive study on the mechanical behaviour of composite laminated plates undergoing a low-speed impact of an external body while they are subjected to in-plane preloads. The effect of such preloading was investigated by means of finite-element analysis of several impact events on laminates with three different span-to-thickness ratios. Tensile and compressive preloads, both uniaxial and biaxial, were considered; in the case of compression, the impact on buckled specimens was also studied. The results obtained show that the span-to-thickness ratio is a fundamental parameter in determining the effect of initial strains. Under a tensile preload, the impact-caused peak stresses were higher than in the case of no preload, and their increment was higher in thicker laminates. Under compression, the most dangerous influence of initial stresses was found at medium span-to-thickness ratios for preloads comparable with the buckling load, whereas, in other cases, negligible or even beneficial effects were observed. These results can justify some experimental findings from the existing literature, even if they were obtained without modelling the material degradation due to damage. Also, they allow us to conclude that the explanation of other phenomena strictly related to damage, as well as an accurate prediction of the extent of damage, requires a failure model.

1. Introduction

During the last few decades, the damage caused by a low-speed impact of foreign objects on composite laminates has been considered as the major threat for the safety of structural components made of these materials. Of special concern are the internal delaminations, because they can lead to a significant reduction in the laminate strength, particularly under compressive loading, but they may be left undetected [1].

Most of the research papers published to date deal with a low-speed impact response and with the material damage of laminates that are free from in-plane preloads. Although it is far more likely that the structural components are impacted while they are subjected to some load during service, only a few contributions dealing with the influence of such preloads on the transient behaviour and failure mechanisms of laminates are available [2-15]. It should also be noted that some loading conditions are less investigated than others. For instance, to the best of our knowledge, [12, 13] are the only experimental studies on

Department of Mechanical Engineering (DIEM) Alma Mater Studiorum – Universita di Bologna viale Risorgimento, 2 – 40136 Bologna, Italy. Russian translation published in Mekhanika Kompozitnykh Materialov, Vol. 46, No. 3, pp. 431-458, May-June, 2010. Original article submitted November 24, 2009.

Corresponding author; tel.: +390512093266; fax: +390512093412; e-mail: giangiacomo.minak@unibo.it .

0191-5665/10/4603-0299 © 2010 Springer Science+Business Media, Inc.

biaxially preloaded continuous-fibre composites; impact tests under compressive preloads are reported only in [8, 9, 11], and [11] is the only experimental research focused on a low-speed impact on laminates buckled in compression. The difficulties encountered in laboratory tests of this kind (machines able to apply very high forces to the specimens are needed [12]) are a probable justification for the apparent little interest in this topic.

According to numerical calculations carried out by several authors, the tensile prestress tends to induce a stiffer impact response, with smaller laminate displacements, a shorter contact duration, larger vibration frequencies, and a higher contact force than in the case of no preload [2, 5, 6, 14, 15]. Compressive loads cause opposite effects, as long as they are lower than the critical buckling load [5, 6, 15]; in postbuckling conditions, a stiffer behaviour is found again, because the buckled laminate acts as a shell, and significant membrane forces are generated as a consequence of deflection [4]. Tensile preloads decrease the transient part of stresses (or strains), while compressive ones increase it [2, 5, 6]; when the overall stresses are considered, an increment is observed both under compression and under tension [15]. However, the changes in stresses and contact forces due to a preload do not seem to have the same importance in different cases; no clear tendency is found regarding the stresses in buckled laminates under impact loads [4].

Experimental tests partly confirm these trends, but the influence of in-plane loads on material damage does not appear to follow definite rules. For example, both wider and smaller delamination areas are found after an impact under tensile preloads, depending on test conditions [7, 9, 10]; a reduction in the threshold impact energy required to produce incipient damage is reported in some cases [10], but this was not observed in other instances [9]. As regards the compressive prestresses, the most detrimental effects of preload seem to take place when the buckling load and the compressive strength of a laminate are close to each other, but only one paper is concerned with this point [11]. The possibility of catastrophic failure during an impact when a compressive load is applied is also reported in [11].

It appears from the brief literature review that the available information is far from providing a complete understanding of the subject, mainly because the validity of the results obtained in each single research may often be limited to the particular conditions examined in it. Besides, in many experimental studies, some important pieces of information concerning the test configuration adopted (e. g., specimen dimensions and layup, material properties, and impact parameters) are missing, thus making the interpretation of the results more difficult. Finally, dissimilar research approaches often focus on different test parameters, preventing a direct comparison between their conclusions. In our opinion, there is a need for a more comprehensive investigation which should be able to assess some general guidelines, especially on the variation of the effect of membrane preloads on the impact behaviour when the main test parameters are changed.

Our previous research on the dependence of impact behaviour and damage of unloaded laminates on specimen dimensions [16], together with several preliminary numerical analyses, suggested that the laminate span-to-thickness ratio could have a fundamental role in determining the influence of preloads on its dynamic response. Accordingly, a number of low-speed impact simulations were performed for composite laminated plates with different in-plane dimensions, but with equal thickness. Various preload conditions, including both tension and compression, uniaxial and biaxial, were examined; regarding compressive preloads, the case of impact on buckled plates was also considered. Particular attention was paid to the comparison of maximum stresses obtained in each case.

The numerical model used for the analyses included the geometrical nonlinearity, because the effect of large deflections proved to be crucial in explaining how the impact behaviour was affected by in-plane forces. On the other hand, no damage model of the material was implemented. By comparison of present numerical results with experimental findings described in the literature, this choice made it possible to distinguish between phenomena which can be justified without account for material degradation and phenomena whose explanation does require a failure model.

The results of the present study show that the in-plane dimensions of an impacted laminate relative to its thickness actually represent a critical parameter. A tensile preload can increase the maximum stresses and lower the impact energy threshold necessary to induce a first damage; however, this effect is much stronger at small span-to-thickness ratios and becomes less and less important as the ratio increases. On the other hand, compressive in-plane loads exhibit beneficial effects at small span-to-thickness ratios, while they are not significant for very slender plates. Between these extreme conditions, at medium

span-to-thickness ratios, the most dangerous influence of preloads was found. Within this framework, some experimental results from the previous researches can be given a better interpretation, and their significance can be clarified.

2. Main Features of the Numerical Model Used

A transient analysis of the impact response of composite laminates was carried out by means of a finite-element program (written in Fortran 90) previously developed by D. Ghelli [17]. Three- and four-node flat shell finite elements based upon the first-order shear deformation theory were implemented. The standard isoparametric formulation was adopted for in-plane and bending strains, while a special approach [18] was chosen for shear strains in order to reduce the locking phenomena. The geometrical nonlinearity related to large deflections was included in the model according to a total Lagrangian formulation [19]. Only the nonlinear contribution to in-plane strains due to transverse displacements was taken into account; thus, the model implemented is equivalent to the Reissner–Mindlin–von Karman theory for plates undergoing large deflections [20]. After discretization, Newton's second law for the laminate takes the well-known general form

$$\mathbf{M}\ddot{\boldsymbol{\Delta}} + \mathbf{C}\dot{\boldsymbol{\Delta}} + \mathbf{F}^{\mathrm{l}} + \mathbf{F}^{\mathrm{nl}} = \mathbf{R}, \tag{1}$$

where $\mathbf{M}$ is the mass matrix, $\mathbf{C}$ is the viscous damping matrix, $\boldsymbol{\Delta}$ is the vector of nodal degrees of freedom, $\mathbf{R}$ is the external load vector, and $\mathbf{F}^{\mathrm{l}}$ and $\mathbf{F}^{\mathrm{nl}}$ are the linear and nonlinear parts of the internal load vector $\mathbf{F}$.

An explicit numerical time integration of (1) was performed by using the central difference scheme [19], which leads to the system of linear algebraic equations

$$\left(\frac{\mathbf{M}}{h^2} + \frac{\mathbf{C}}{2h}\right)\boldsymbol{\Delta}(t+h) = \mathbf{R}(t) - \mathbf{F}(t) + \frac{2\mathbf{M}}{h^2}\boldsymbol{\Delta}(t) + \left(\frac{\mathbf{C}}{2h} - \frac{\mathbf{M}}{h^2}\right)\boldsymbol{\Delta}(t-h) \tag{2}$$

for every discrete instant t, where h is the time step. This system must be solved for the unknowns $\Delta(t+h)$. The lumped (diagonal) mass and damping matrices were employed so that the equations in (2) are uncoupled. Further details on the implementation of the numerical model can be found in [17]. During the analysis of impact events, the matrix $\mathbf{C}$ was set to zero, thus no damping effect was considered; $\mathbf{C}$ was used only in the dynamic relaxation algorithm (see below).

The impactor was treated as a rigid body. The contact between the impactor and the target was modelled in a simplified way, by applying the contact force as an external load to a single node of the discretized laminate. Following a generally accepted approach [1], a Hertz-type contact law was assumed to be valid:

$$P = k\alpha^{3/2},$$

where P is the contact force and α is the indentation of the impactor in the laminate surface.

The contact and large deflections were the only nonlinear phenomena accounted for in the numerical model. In particular, no postfailure degradation criterion of material properties was implemented, so that the elastic constants did not change during the simulations even if failure was predicted. This simplifying assumption makes it possible to obtain reliable results as long as the actual material damage is limited [16]; the parameters of the impact events studied herein were therefore suitably chosen in order to meet this condition.

In addition to the features summarized so far and described in [17], a dynamic relaxation technique was included in the program for purposes of the present study. This technique enables one to use the same code developed for a transient analysis to find the solution of a static problem and is known to be very simple and efficient in circumstances where strong nonlinear effects, like those related to the elastic instability, are present [21]. For these reasons, it was adopted to evaluate the postbuckling configuration of the laminates subjected to in-plane compression.

If constant external loads are applied and an artificial viscous damping is introduced, the transient solution of system (1) converges to its steady-state part, which satisfies the equilibrium equations

$$\mathbf{F}^{\mathrm{l}} + \mathbf{F}^{\mathrm{nl}} = \mathbf{R}.$$

Since, in this case, the aim of the explicit analysis is to find a static solution, which depends only on the internal load vector **F**, while the transient part of the solution is not of interest, the mass matrix **M** need not contain the real inertial properties of the structure. In the present study, during the dynamic relaxation calculations, the elements of **M** were given fictitious values, obtained with a procedure based upon Gershgorin's circle theorem, which improves the computational efficiency of the algorithm [21]. The damping matrix **C** was set proportional to **M**, so that both the matrices were diagonal; the ratio between the elements of **C** and **M** was adjusted in order to approximate the condition of critical damping for the first (fictitious) vibration mode, because in this way the number of iterations required for convergence is the lowest [21].

2.1. Choice of case studies. For the present study, a simple square laminated plate was chosen as the target structure subjected to an impact. In order to elucidate how the effect of preload on the impact response varies in relation to the test conditions, three different in-plane dimensions were considered: 25, 100, and 400 mm. From here on, they will also be referred to as small, medium, and large laminates, respectively. The laminate thickness of 2.13 mm was kept constant in all cases, thus obtaining three different values of span-to-thickness ratio: 11.8, 47.0, and 188. The first and third ones were intended to represent two opposite limiting configurations (very thick and very slender plates); the second one was chosen to reproduce intermediate conditions.

The laminates considered consist of 16 graphite-epoxy unidirectional plies arranged in the symmetric quasi-isotropic layup $[(45/0/–45/90)_s]_2$. For the elastic constants (E_1 = 148 GPa, E_2 = 9.58 GPa, G_{12} = G_{13} = 5.61 GPa, G_{23} = 3.0 GPa, ν_{12} = 0.287) and in-plane strengths (X_t = 1630 MPa, X_c = 1290 MPa, Y_t = 45.6 MPa, Y_c = 216 MPa, S = 150 MPa) of the single lamina, as well as for the thickness and stacking sequence of the laminate, the values given in [10] were adopted ([10] was chosen among the cited references because it provides the most complete information about the mechanical properties of the specimens). However, for the present simulations, the choice of their absolute values was not essential (of course, they had to be realistic), the final aim being the study of the influence of other parameters, such as the preload and the span-to-thickness ratio.

The mass density was assumed to be 1580 kg/m^{-3}, a common value for graphite-epoxy. The contact stiffness k was determined from the formula used by Yang and Sun [22]

$$k = \frac{4}{3} \cdot \frac{\sqrt{R_s}}{\dfrac{1-\nu_s^2}{E_s} + \dfrac{1}{E_2}},$$

where E_s and ν_s are Young's modulus and the Poisson ratio of the impactor material, and R_s is the radius of curvature of the impactor head. R_s was given the value of 6.35 mm, typical of many drop-weight experimental devices; regarding the head as made of steel, E_s = 210 GPa and ν_s = 0.3. These assumptions yield $k = 9.78 \cdot 10^8$ N $\cdot$ m$^{-3/2}$.

In all impact testers able to apply in-plane loads to the specimens, clamping devices are needed to grip their ends properly; rotation is thus prevented along the boundary of the unrestrained area. Even if the servohydraulic preloading apparatus is intended to accomplish a fixed displacement or fixed strain condition, as explicitly stated in some cases [12, 13], it is not possible to ascertain to what extent this ideal limit is approached during impact tests. The actual boundary condition is most likely neither a fixed load nor a fixed displacement; however, it is likely to be much closer to the latter one. Therefore, all degrees of freedom along the plate boundary were constrained in the present numerical analyses, thus simulating full clamping conditions.

The initial velocity of the impactor was normal to the plate surface, and the contact occurred exactly at the plate centre. As a reference for the subsequent calculations including a membrane preload, one impact analysis was performed without a preload for each of the three aforementioned laminate dimensions. The initial energy of the impactor in these analyses was chosen so that the material damage expected was limited, in order to ensure that the present results, obtained without a damage model, are reliable. To verify this, the Tsai–Wu failure criterion [23] was applied to each lamina; the maximum values of the failure index attained during the transient response were computed and plotted (examples of these plots can be found in Figs. 2a, 4a, and 6a). By using the trial-and-error method, we found the impact energy resulting in a small area where the index exceeded the threshold value 1 (corresponding to failure) in the lamina subjected to the highest stresses. By checking the stress components, it was concluded that the failure predicted should be the matrix cracking in tension. For a 6.8-kg impactor (as in

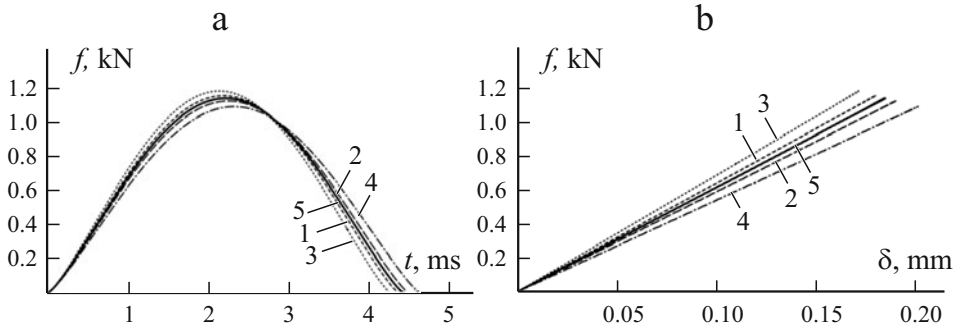

Fig. 1. Contact force f as a functions of time t (a) and displacement δ (b) for the 25-mm laminate impacted under uniaxial (1, 2) and biaxial (3, 4) prestrains of magnitude $2400 \cdot 10^{-6}$: tensile (1, 3), compressive (2, 4), and with no preload (5).

[10]), the initial speeds corresponding to this "small damage" condition were evaluated as 0.20, 0.45, and 1.8 m/s for the small, medium, and large laminates, respectively. At such a low speed, the impact response is dominated by the first vibration mode; this allows the best understanding of the influence of preload, as will be shown later. The effect of various impact speeds will also be investigated separately.

3. Tensile Preload

3.1. Case studies. The impact events considered in studying the tensile preloads were as follows. The initial strain of $2400 \cdot 10^{-6}$, the highest among the three examined in [10], was considered representative of common service conditions of composite laminates. In a first set of simulations, aimed at evaluating the influence of in-plane loads for specimens of different dimensions, an impactor of mass 6.8 kg was used in all cases; the initial speeds of the impactor were 0.20, 0.45, and 1.8 m/s for the 25-mm, 100-mm, and 400-mm specimens, respectively, as explained in the preceding section. A second group of simulations was performed in order to investigate how the previous results were affected by a change in the impact speed. These analyses concerned only the large laminates, for which the effect of speed was found to be most significant. In this group, the mass of the impactor was reduced by 4 and 16 times as the speed was increased to the new values of 3.6 and 7.2 m/s, respectively, so that the initial energy was the same in all cases. This ensured that the condition of small damage area was maintained.

The in-plane load was imposed on the laminates in the form of initial displacements of nodes. It has to be noted that, even if the preload is expressed in terms of strain, "uniaxial" refers to the load, not to strains. In other words, the initial condition of the laminate under a uniaxial preload was obtained by imposing a specified strain value in the loading direction, while the material was free to shrink in the orthogonal direction due to the Poisson effect, as would happen in a test machine when a uniaxial loading is required. In the case of a biaxial prestrain, equal strains in two perpendicular directions were applied; this also led to equal force resultants in all directions, since the laminate was quasi-isotropic.

The discretizations to be used were chosen after a convergence test for each of the three laminate dimensions considered. The small specimen was discretized with a uniform mesh of 256 (16 by 16) square four-node finite elements. The medium and large laminates required 1024 (32 by 32) elements for sufficiently accurate results. In the central difference algorithm, the time integration step h must be lower than the critical stability threshold, because the method is stable conditionally [19]. In the present analyses, h was equal to 0.2 μs for the small, 0.4 μs for the medium, and 0.7 μs for the large laminates.

3.2. Results. The results of the first set of simulations (with the same impactor mass) are presented in Figs. 1-6. The history of contact force for impacts on the 25-mm laminate subjected to different preloads is plotted in Fig. 1a. Figure 1b shows the contact force f as a function of displacement δ of the node on which the impact occurs. Analogous graphs are plotted in

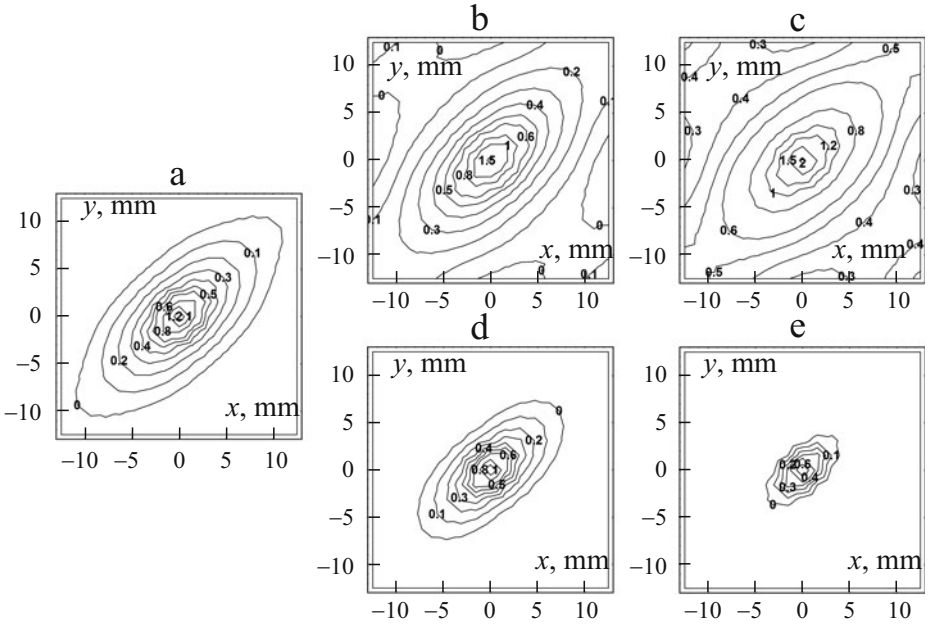

Fig. 2. Tsai–Wu failure index for the 25-mm laminate impacted under no preload (a) and under uniaxial tensile (b) and compressive (d) and biaxial tensile (c) and compressive (e) prestrains of magnitude $2400 \cdot 10^{-6}$.

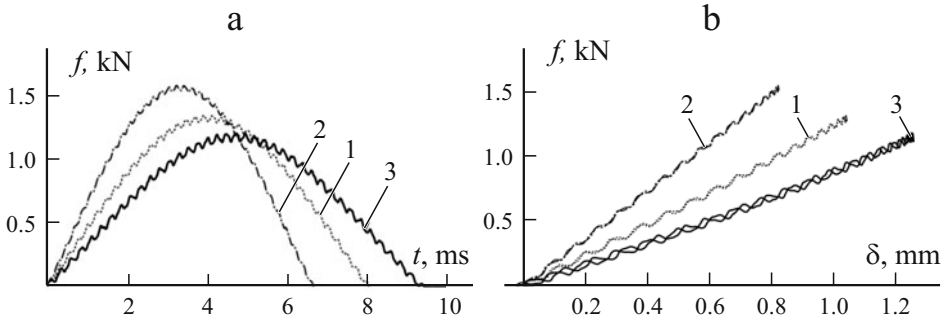

Fig. 3. Contact force f as functions of time t (a) and displacement δ (b) for the 100-mm laminate impacted under uniaxial (1) and biaxial (2) tensile prestrains of magnitude $2400 \cdot 10^{-6}$ and under no preload (3).

Figs. 3 and 5 for the 100-mm and 400-mm specimens, respectively. The numerical values of the maximum contact force, the maximum displacement of the impactor, and the contact duration in all the test conditions considered are collected in Table 1.

In Fig. 2, the plots of the Tsai–Wu failure index are compared for the cases of impact, without a preload and under uniaxial and biaxial preloads on the small specimens. The same for the medium and large specimens is shown in Figs. 4 and 6, respectively. In all cases, the highest values of the index were recorded in the lowermost ply, on the side opposite to the impacted surface of the laminate. Therefore, all the pictures refer to this ply and to the time when the overall stress state was the most severe during the transient response.

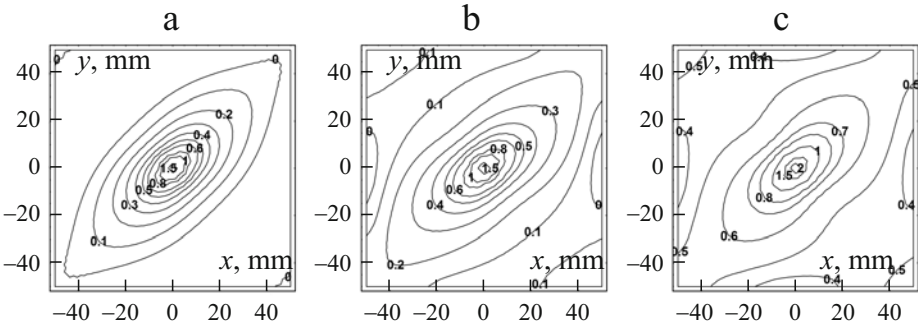

Fig. 4. Tsai–Wu failure index for the 100-mm laminate impacted under no preload (a) and under uniaxial (b) and biaxial (c) tensile prestrains of magnitude $2400 \cdot 10^{-6}$.

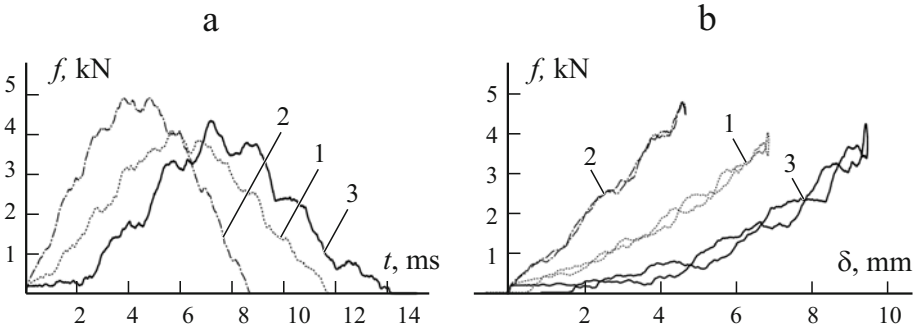

Fig. 5. Contact force f as functions of time t (a) and displacement δ (b) for the 400-mm laminate impacted under different preloads. Designations as in Fig. 3.

The results of the second set of simulations, regarding the influence of different impact speeds, but for the same initial kinetic energy of the impactor, are presented in Figs. 7 and 8. Figure 7 shows the contact force, the displacement of impactor, and the deflection of the impacted node as functions of time t for the unloaded laminate at different impact speeds. Figure 8 displays the effect of membrane load on the history of contact force for different impact speeds. The numerical values of the most important relevant parameters are reported in Table 2.

3.3. Discussion. In an attempt to comment on the results of the numerical simulations presented above, it is convenient to start from the impact events at the lowest impact speed (Figs. 1-6). In these cases, the dynamic response of the laminate is dominated by the fundamental vibration mode: the contribution of higher modes is either small (for the 100-mm and 400-mm specimens), as can be seen from the minor secondary oscillations in the history of contact force in Figs. 3 and 5, or negligible (see Fig. 1). In this situation, the transient behaviour of the target can be viewed as a succession of quasi-static equilibrium states, and therefore the explanation of some features of the response is greatly simplified.

In the 25-mm specimen, owing to its high stiffness, the first failure is reached at very small transverse displacements. As a consequence, the membrane stiffening due to the immovable edges has a negligible effect on the load–displacement curve, which does not show any deviation from linearity (see Fig. 1b). Since the influence of preload is strictly related to the geometrical nonlinearity, it is expected that little differences exist between the unloaded and preloaded specimens. This is exactly what is seen from the plots in Fig. 1, showing that the dynamic behaviour of the small laminate is almost unaffected by in-plane loads. On the other hand, the stresses in the preloaded laminates exhibit a definite increase with respect to those in the unloaded condition (see Fig. 2). This is easily explained bearing in mind that, in a quasi-static configuration, the part of stresses due to bending depends on the deflection (in fact, the peak stresses are attained approximately at the instant of maximum deflection),

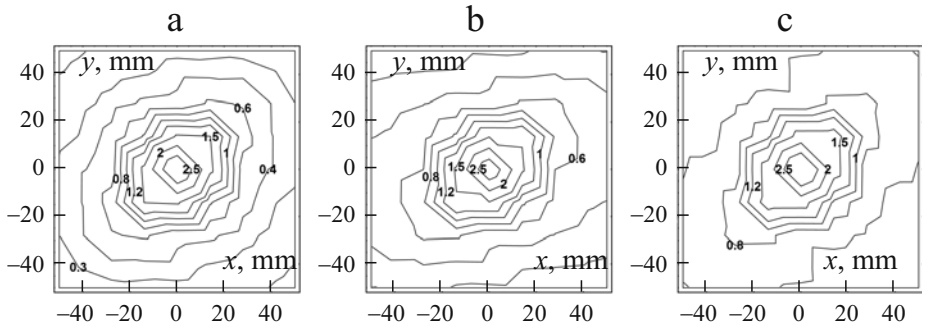

Fig. 6. Tsai–Wu failure index for the central zone of the 400-mm laminate impacted under different preloads. Designations as in Fig. 4.

TABLE 1. The Contact Force f, Impactor Displacement δ, and Contact Duration t for Impacted Laminates of Different Length

Laminate length, mm	Characteristic	With no preload	Initial strain $2400 \cdot 10^{-6}$	
			Uniaxial	Biaxial
25	f, kN	1.145	1.160	1.188
	δ, mm	0.295	0.291	0.285
	t, ms	4.40	4.34	4.24
100	f, kN	1.23	1.38	1.62
	δ, mm	1.40	1.19	0.983
	t, ms	9.43	8.06	6.68
400	f, kN	4.32	4.09	4.90
	δ, mm	9.85	7.20	5.01
	t, ms	14.1	11.7	8.62

which is left unchanged by the preload. Therefore, the overall stress state is approximately a direct superposition of the pre-existing stresses on the bending stresses, the former representing a significant contribution.

Moving to the 100-mm and 400-mm laminates, it can be noted that the influence of preload becomes more and more significant as regards the dynamic response: the contact duration is shortened, the maximum force tends to grow, and the maximum displacement diminishes. On the contrary, in the medium laminates, the increase in stresses due to preload is lower than in the small ones and becomes almost invisible in the large plates. The evident curvature of the force–displacement paths in Fig. 3b and 5b indicates that the geometrical nonlinearity plays an important role in limiting the deflection of the plate; of course, this phenomenon is more significant at higher span-to-thickness ratios. Therefore, the overall stress state in the preloaded laminates is no longer the result of superposition of pre-stresses on bending stresses of the unloaded specimen. The bending stresses are reduced due to smaller deflections (as found in previous studies [2, 5, 6, 15]) as the membrane forces are increased, and it is not possible to say a priori which effect will prevail. The present analyses show that, in low-speed impacts, the total stresses are higher when membrane preloads are applied; however, the difference with respect to those in the unloaded condition strongly depends on the span-to-thickness ratio of the target and tends to disappear in very slender laminates, whose behaviour resembles that of a membrane.

Regarding the impact dynamics, the trends described above agree with conclusions of other numerical analyses [2, 5, 6, 15]. The results of experimental tests partly confirm the theoretical predictions. When the influence of a preload is recog-

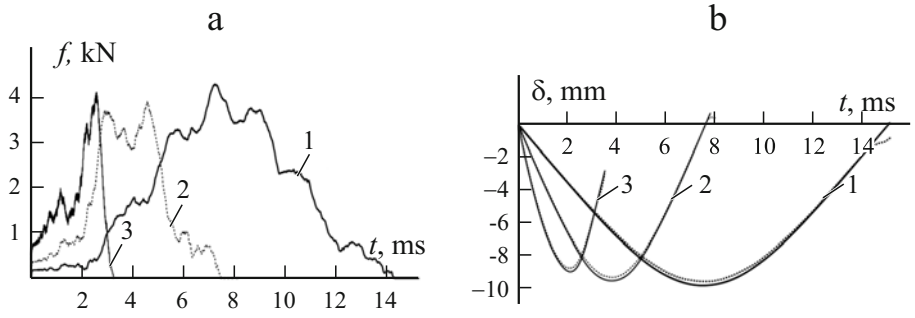

Fig. 7. The contact force f (a) and displacement δ (b) as a functions of time t for the 400-mm laminate impacted at speeds of 1.8 (1), 3.6 (2), and 7.2 m/s (3) under no preload; (——) — impactor displacements and (- - -) — target displacements.

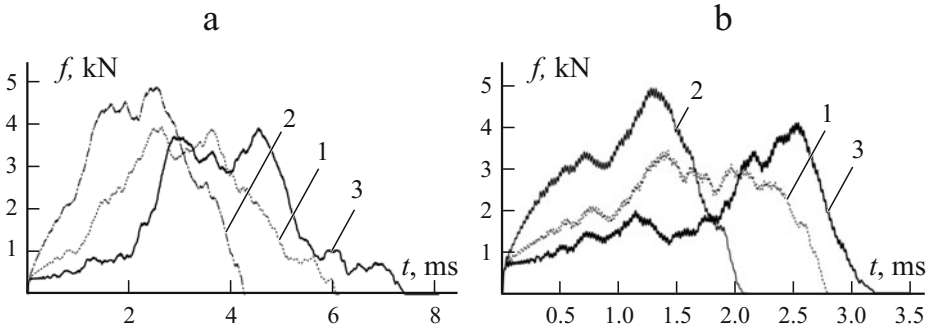

Fig. 8. History of contact force f for the 400-mm laminates impacted at 3.6 (a) and 7.2 m/s (b) with the same initial energy under uniaxial (1) and biaxial (2) tensile prestrains of magnitude $2400 \cdot 10^{-6}$ and under no preload (3).

nized, it generally consists in a stiffer response of the target, with a shorter contact duration and a higher force [8-10, 12, 13]. However, the effect of preload on the maximum contact force is often small, sometimes negligible. In view of the present results, this could be due to the span-to-thickness ratio. Unfortunately, this parameter is hardly ever provided in the available reports of experimental studies. In [8], specimens with a span-to-thickness ratio of 36.8 are tested, so a difference even less pronounced than that seen in Fig. 3 is expected; this is exactly what the plots of contact force history in [8] display. In [12, 13], the ratio is higher (84.3 and 71.1, respectively), but the effect of prestrain on the contact force is hardly visible. However, this seeming contradiction with the present study may be explained by the low level of prestrain (within $1500 \cdot 10^{-6}$). Other important factors which can obscure the influence of preload are the experimental data scatter (which alone could easily hide differences like those in Figs. 1 or 3) and material damage, which alters the history of contact force, lowering the highest peaks predicted by a numerical simulation without a damage model and extending the contact duration [16]. This is most likely true with respect to [12], where significant damage was introduced, as far as perforation of the laminate.

The extent of the damaged area, especially if very large, cannot be reliably predicted by an analysis which does not take into account material degradation [16]. Consequently, it is not possible to deduce from, for instance, Fig. 2 that a larger damaged zone is expected in the small preloaded laminates. These pictures are also relevant to the stress state within a lamina, thus they cannot be used to predict a delamination, which is the form of damage usually detected after impact tests and referred to as “damaged area”. As regards this parameter, conflicting results are reported in the literature. According to [8], in short-fibre composites, the damage area is left practically unchanged by a biaxial preload, while a uniaxial tensile prestress can in-

TABLE 2. Values of f, δ, and t for the 400-mm Laminate Subjected to Different Impact Speeds

Impact speed, m/s	Characteristic	With no preload	Initial strain $2400 \cdot 10^{-6}$	
			Uniaxial	Biaxial
1.8	f, kN	4.32	4.09	4.90
	δ, mm	9.85	7.20	5.01
	t, ms	14.1	11.7	8.62
3.6	f, kN	3.92	3.96	4.89
	δ, mm	9.55	7.06	4.92
	t, ms	7.42	6.03	4.23
7.2	f, kN	4.14	3.48	5.00
	δ, mm	9.00	6.78	4.80
	t, ms	3.20	2.80	2.07

Fig. 9. Deformed shape of the 400-mm laminate after a 7.2-m/s impact in the absence of preload.

crease it. In [10], opposite effects are described for laminates of different thickness; a dependence on the impact energy is also found to exist. In [9], larger delaminations with uniaxial in-plane loads were observed, while in [13] no difference existed between unloaded and biaxially preloaded specimens, maybe because of the small initial strain. These findings, contrasting with the present simulations showing generally a more severe stress state under preload, suggest that the implementation of a failure model is required to predict the extent of damage.

Instead, an important conclusion can be drawn concerning the impact energy threshold which initiates damage. The graphs in Figs. 2, 4, and 6 show that, the impact energy being the same, the stresses are higher under an initial membrane load. Therefore, it is expected that a lower impact energy is required to induce a first damage under a preload; the difference with respect to the laminate free from prestress will be larger for thicker plates. Only three papers present results concerning the impact energy threshold, probably because the evaluation of this parameter is quite expensive (many tests at several energy levels are needed); unfortunately, the span-to-thickness ratio of the coupons is never indicated. In [7], the preload is found to decrease the energy threshold, but for beam-like specimens impacted at a medium speed (10-40 $m \cdot s^{-1}$). In [9], the threshold does not seem to be sensitive to the preload, whereas in [10] it diminishes in every test condition. In any case, the present results suggest that the possible future studies should investigate the relationship between the energy threshold and the span-to-thickness ratio experimentally.

Figures 7 and 8 indicate how the guidelines discussed so far are affected by higher impact speeds. Keeping the impact energy constant results in the maximum force and the maximum deflection approximately equal to those at the lowest impact speed. The peak stresses (not shown here) also remain similar to those displayed in Fig. 6. Figure 7 shows that the history of contact force becomes more and more irregular, because the contribution of higher vibration modes is no longer negligible. The dynamic response cannot be considered as a succession of quasi-static equilibrium states, since it is governed by wave propagation phenomena, clearly distinguishable in the deformed shape of plate plotted in Fig. 9. These effects are more evident in a

TABLE 3. Compressive Preloading of Laminates

Preload	Laminate length, mm		
	25	100	400
Uniaxial	$-2400 \cdot 10^{-6}$	$0.50\varepsilon_{cr}$. $0{,}90\varepsilon_{cr}$	$0.50N_{cr}$, $0.90N_{cr}$, $1.07N_{cr}$ ($1.10N_{cr}$), $1.35N_{cr}$ ($1.50N_{cr}$), $1.67N_{cr}$ ($2.00N_{cr}$), $1.99N_{cr}$ ($3.00N_{cr}$)
Biaxial	$-2400 \cdot 10^{-6}$	$0.50\varepsilon_{cr}$, $0.90\varepsilon_{cr}$, $1.05\varepsilon_{cr}$ ($1.10\varepsilon_{cr}$), $1.24\varepsilon_{cr}$ ($1.50\varepsilon_{cr}$)	$0.50N_{cr}$, $0.90N_{cr}$, $1.05N_{cr}$ ($1.10N_{cr}$), $1.25N_{cr}$ ($1.50N_{cr}$), $1.48N_{cr}$ ($2.00N_{cr}$), $1.93N_{cr}$ ($3.00N_{cr}$)

TABLE 4. Values of f, δ, and t for the 25-mm Laminate Impacted under a $2400 \cdot 10^{-6}$ Compressive Prestrain

Prestrain	f, kN	δ, mm	t, ms
No	1.145	0.295	4.40
Uniaxial	1.129	0.299	4.47
Biaxial	1.096	0.309	4.60

larger laminate, where it takes longer for the waves to reach the boundary and be reflected back; for this reason, the 400-mm specimen was chosen here to highlight them.

A general rule concerning biaxial preloads emerges from the results. In every test configuration, a biaxial initial load has much stronger influence both on the impact response and on stresses than a uniaxial one. To a certain extent, this also holds when the speed is not so low (see Fig. 8).

However, Fig. 8 suggests that the trends found for low-speed impacts tend to lose their validity when the speed is increased; for instance, the maximum force under a uniaxial prestrain can be lower than in the unloaded case (see Fig. 8b). Localized peaks of contact force may induce the maximum stresses and are of great importance. In the conditions simulated here for the large laminate, their effect on stresses is likely limited, as mentioned above; this agrees with the results obtained in [14] for an infinite plate. Nevertheless, for even higher speeds, a wave-dominated response can also be obtained in smaller plates, where the influence of preload proved to be more significant. In such circumstances the danger created by a preload cannot be quantified a priori, and a suitable calculation is necessary for any specific case to be examined.

4. Compressive Preload

4.1. Case studies. Table 3 contains the data of all impact tests simulated for studying compressive preloads. The initial speed of impactor was the same as in the first set of analyses, performed under a tensile prestrain; the impactor mass was kept equal to 6.8 kg in all cases, and thus the corresponding kinetic energy was assumed the same as in the case of tensile preload. The discretizations and time steps used were identical to those chosen for the previous simulations.

In the small specimen, no instability phenomenon was predicted by the dynamic relaxation analysis, even at very high prestrain levels which would most likely cause failure of the laminate in practice; of course, this is due to the low span-to-thickness ratio. For this reason, the critical load was not evaluated, and the preload was expressed in terms of strain and given the same absolute value already used for the tensile preload. This specimen dimension was intended to reproduce the limiting condition in which damage is not influenced by the global elastic instability.

TABLE 5. Values of f, δ, and t for the 100-mm Laminate Impacted under Different Compressive Preloads at a Speed of 0.45 m/s

Preload		f_{max}, kN	δ_{max}, mm	t, ms
No		1.23	1.40	9.43
$0.50N_{cr}$	Uniaxial	1.13	1.75	11.3
	Biaxial	1.13	1.77	11.3
$0.90N_{cr}$	Uniaxial	1.22	2.31	13.7
	Biaxial	1.21	2.32	13.7
$1.05N_{cr}$	Biaxial	1.31	1.76	10.7
$1.24N_{cr}$	Biaxial	1.50	1.22	8.00

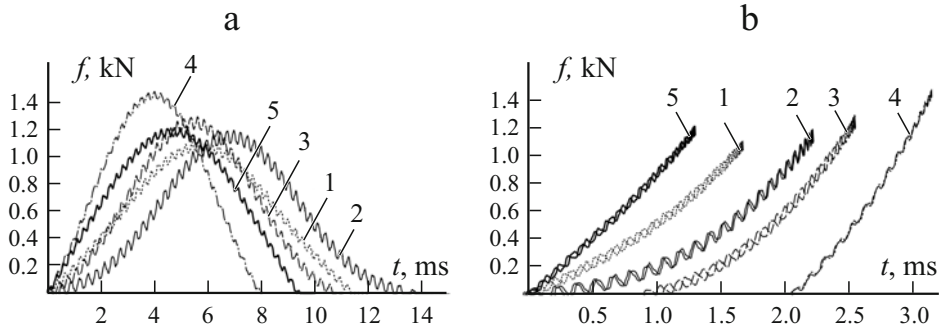

Fig. 10. Contact force f as functions of time t (a) and displacement δ (b) for the 100-mm laminate impacted under compressive preloads of $0.50N_{cr}$ (1), $0.90N_{cr}$ (2), $1.05N_{cr}$ (3), and $1.24N_{cr}$ (4) and under no preload (5).

In the medium and large laminates, the buckling was predicted by numerical calculations to occur at lower strains (within $4000 \cdot 10^{-6}$); these cases can therefore represent more common situations in practical applications, where the allowable stresses are dictated by instability, because the true compressive strength of the material (measured by using test devices preventing buckling) cannot be reached. For these laminates, the first critical loads, both uniaxial and biaxial, were evaluated numerically together with the corresponding strains, and the values of initial in-plane load to be tested were expressed as fractions of the critical load N_{cr}.

As for the analysis of tensile membrane forces, the compressive preload was applied through displacements imposed on the nodes of the finite-element model, and the term "uniaxial" means a uniaxial load (not a strain) wherever used. In determining the postbuckling shape of the laminates, their boundary was constrained to maintain its rectangular shape, in order to reproduce the usual experimental configuration where the specimen sides are clamped. This means that equal displacements were imposed on all nodes of each side in the direction perpendicular to the boundary. Obviously, the resulting in-plane forces are not constant along the boundary; therefore, the fractions of N_{cr} were calculated as average values over the entire side length. When larger than unity, the fractions of the critical strain ε_{cr} refer to an ideal planar configuration of the plate (loaded beyond the critical level), used as the initial condition of the dynamic relaxation analysis which served to find the postbuckling shape. In impact simulations, the postbuckling displacements represented the initial condition of the target, with the same boundary constraints as in the previous dynamic relaxation analysis. For the sake of brevity, only impacts on the concave face of the buckled laminates were considered.

4.2. Results. The force–time and force–displacement diagrams for the 25-mm laminate under compression are shown in Fig. 1; Fig. 2d,e presents plots of the Tsai–Wu failure index. The relevant main parameters are listed in Table 4.

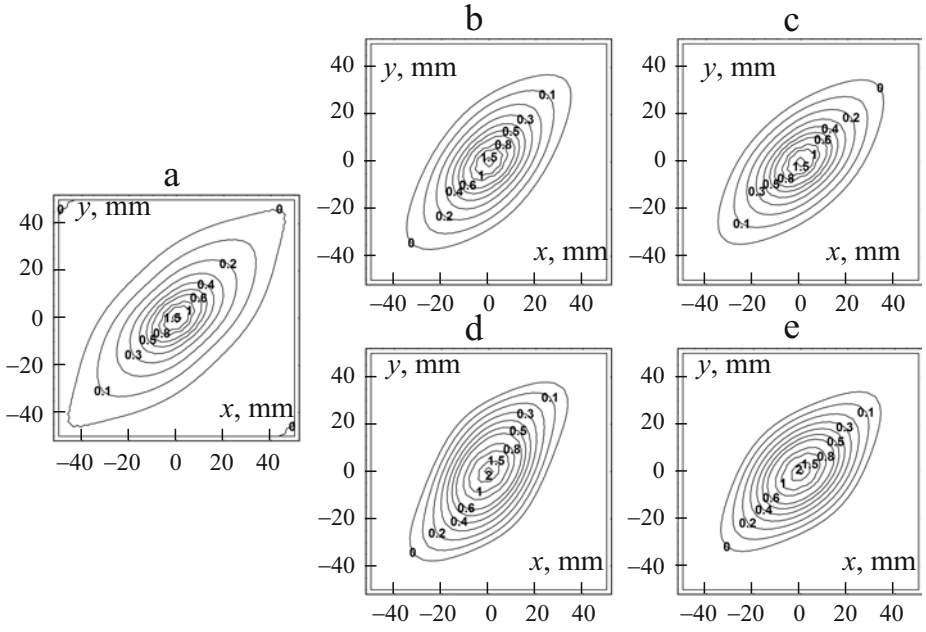

Fig. 12. Tsai–Wu failure index for the 100-mm laminate impacted under no preload (a) and under uniaxial (a, c) and biaxial (b, d) compressive preloads of $0.50N_{cr}$ (b, c) and $0.90N_{cr}$ (d, e).

The critical strains of the 100-mm laminate were $3950 \cdot 10^{-6}$ and $1450 \cdot 10^{-6}$ under uniaxial and biaxial preloads, respectively; the corresponding force resultants were 480 and 253 kN/m. In the postbuckling configuration under uniaxial compression, the stresses on the convex surface of the laminate exceeded the level of first failure: for this reason, no impact test was carried out in this condition. The same happened with the biaxial compression, but only beyond $1.50\ \varepsilon_{cr}$.

Figure 10 shows the history of contact force and force–displacement curves for all tested values of biaxial preload considered. As can be seen from the numerical values in Table 5, in the cases of $0.50N_{cr}$ and $0.90N_{cr}$, the uniaxial and biaxial prestrains gave practically identical results as regards the impact response, and therefore only the curves regarding the latter case have been plotted. The diagrams of the Tsai–Wu failure index are presented in Figs. 11 (for preloads below the critical values) and 12 (for the buckled laminate under biaxial preloads).

The critical strains of the 400-mm laminate were $258 \cdot 10^{-6}$ (uniaxial) and $94 \cdot 10^{-6}$ (biaxial); the corresponding in-plane forces were 31.3 and 16.4 kN/m, respectively. In all the postbuckling configurations examined, the stresses were far below the in-plane strengths of the material. In Fig. 13, the contact force is plotted as functions of time and deflection for biaxial preloads lower than the critical load; as in Fig. 10, the curves obtained for uniaxial initial strains are not displayed, because they are hardly distinguishable from the others. The relevant Tsai–Wu plots are collected in Fig. 14. For all the case studies regarding the buckled laminates, the histories of contact force are presented in Fig. 15. The numerical values of maximum contact force, maximum deflection, and contact duration are given in Table 6.

4.3. Discussion. In the small laminate, which is not prone to buckling, the influence of compressive preloads is directly opposite to that of tensile preloads, as can be seen by comparing the curves in Fig. 1 and the Tsai–Wu diagrams in Fig. 2. The change in the impact response (contact force and laminate deflection) is small due to the low span-to-thickness ratio. On the other hand, the stresses appear to be quite sensitive to the initial strain in this condition. The superposition of a compressive load on the bending stresses related to deflection leads to a much less severe stress state. As a consequence, the impact energy threshold associated with a first damage of the material will be significantly increased by the in-plane load.

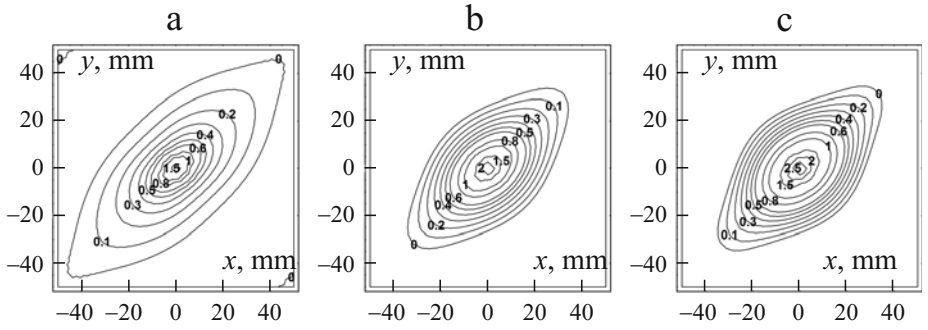

Fig. 12. The same with no preload (a) and under biaxial compressive preloads of $1.05N_{cr}$ (b), and $1.24N_{cr}$ (c).

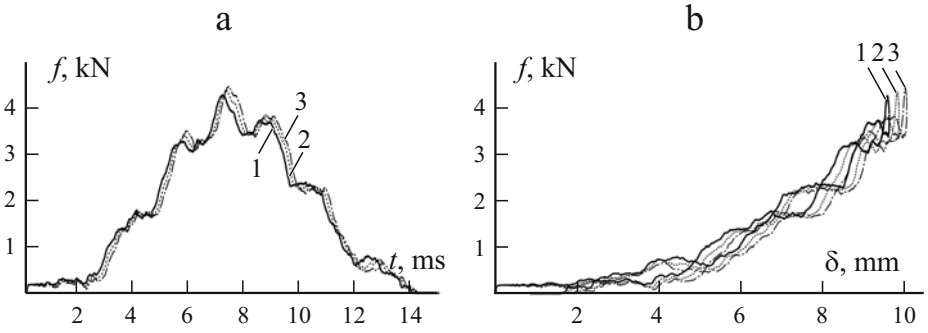

Fig. 13. Contact force f as functions of time t (a) and displacement δ (b) for the 400-mm laminate impacted under no preload (1) and under biaxial compressive preloads of $0.50N_{cr}$ (2) and $0.90N_{cr}$ (3).

It should be mentioned that the Tsai–Wu failure index in Fig. 2d,e, as also in all the other images, refers to the lowermost ply, which is subjected to tension; therefore, it has to be considered as an indicator of possible failure in tension. At the preload level considered, the stress state on the impacted side is far from causing failure in compression. Of course, if the membrane load was increased, the compressive stresses on the uppermost ply would eventually become the most severe and would induce a first damage. However, this situation was not considered in the present study.

The large specimen is subjected to instability at very low in-plane loads. This explains the negligible effect of preloads below the critical values, as regards both the impact dynamics (Fig. 13) and stresses (Fig. 14). Even if a tensile initial strain considerably affects the transient response (see Fig. 5), in Fig. 13 the effect of a compressive preload appears much smaller due to the low absolute values of the applied stress. The Tsai–Wu index for a uniaxial preload (not shown) is practically identical to that calculated under a biaxial preload.

In the previous cases, the contact duration has a tendency to rise because of a preload, but if the in-plane forces exceed the critical load, their influence on the impact behaviour is opposite (see Fig. 15). These trends agree with the results of previous studies, both for specimens preloaded below the critical level [5, 6, 15] and for buckled specimens [4, 11]. In any case, the differences observed here, especially as regards the maximum contact force, are again very small. The same happens for the maximum stresses (no diagram is presented for these cases, because they would repeat those shown in Fig. 14): it can thus be concluded that the impact energy threshold should also not be greatly affected by in-plane loads.

Among the force–time curves in Fig. 15a, it is worth noting the one obtained for the highest preload, which shows a different shape and is associated with a much larger displacement than in other cases (see Table 7). The reason for these peculiarities lies in the mode switching phenomenon occurring under the uniaxial compression between $1.67N_{cr}$ and $1.99N_{cr}$. In

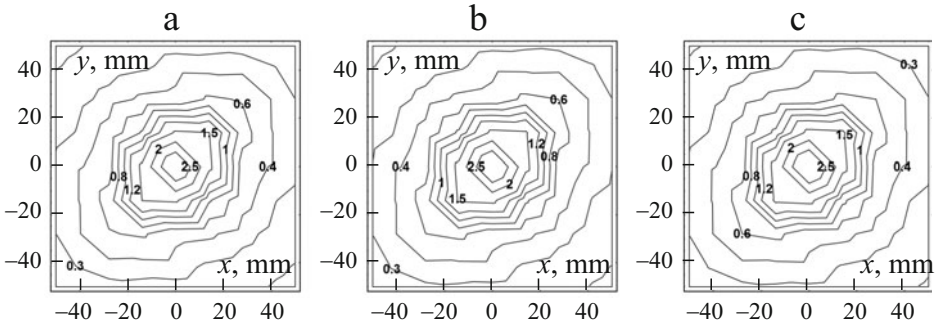

Fig. 14. Tsai–Wu failure index for the central zone of the 400-mm laminate impacted under no preload (a) and under biaxial compressive preloads of $0.50N_{cr}$ (b) and $0.90N_{cr}$ (c).

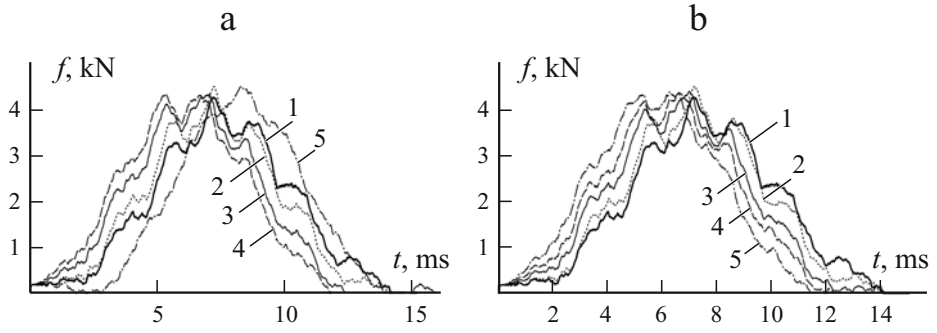

Fig. 15. Contact force f as a function of time t for the 400-mm laminates impacted under no preload (1) and under compressive uniaxial preloads of $1.07N_{cr}$ (2), $1.35N_{cr}$ (3), $1.67N_{cr}$ (4), and $1.99N_{cr}$ (5) (a) and compressive biaxial ones of $1.05N_{cr}$ (2),. $1.25N_{cr}$ (3), $1.48N_{cr}$ (4), and $1.93N_{cr}$ (5) (b).

the latter case, the buckling mode presents two half-waves in the loading direction, whereas in the former one (as in all other cases, including all the examples of biaxial preload) the deformed shape of the buckled specimen has one half-wave in both directions. The response of the laminate buckled into a two-half-wave shape to an impact at its centre (where the initial transverse displacement is zero) is illustrated in Fig. 16. The impactor forces the plate to transform to the first buckling mode; after the rebound, the original second mode is restored, with the two half-waves oscillating back and forth thereafter.

The most interesting situation, with the greatest reduction in the impact energy threshold, takes place in the medium laminate. The impact behaviour is definitely affected by the preload (see Fig. 10); below the critical load, a less stiff response is induced (but the maximum force increases at $0.90N_{cr}$ with respect to that at $0.50N_{cr}$), while, above it, the overall stiffness of the specimen grows quickly, as shown by the slope of the force–displacement curves in Fig. 10b. The stresses exhibit a strong increment when the initial strain, either uniaxial or biaxial, approaches the critical value (Fig. 11), and increase still further in buckled laminates (Fig. 12). Evidently, the higher bending stresses due to larger deflections (with respect to those in the case without a preload) are only partially compensated by superposition of the initial compressive stresses. In addition, in buckled plates, a strong membrane stiffening takes place, which adds a tensile contribution.

This particular combination of conditions can occur only in medium-size laminates. In small laminates, the critical load cannot be reached, and the change in deflection due to a preload is negligible. On the other hand, in large specimens, the deflection might theoretically be strongly affected by a preload (as happens under tension), but actually it is not because the

TABLE 6. Values of f, δ, and t for the 400-mm Laminate Impacted at a Speed of 1.8 m/s under Different Preloads

Preload		f_{max}, kN	δ_{max}, mm	t, ms
No		4.32	9.85	14.1
$0.50N_{cr}$	Uniaxial	4.43	10.08	14.3
	Biaxial	4.43	10.09	14.4
$0.90N_{cr}$	Uniaxia	4.48	10.27	14.8
	Biaxial	4.51	10.28	14.3
$1.07N_{cr}$	Uniaxia	4.56	9.27	14.3
$1.05N_{cr}$	Biaxial	4.55	9.44	14.0
$1.35N_{cr}$	Uniaxiaя	4.39	8.16	15.7
$1.25N_{cr}$	Biaxial	4.45	8.50	14.3
$1.67N_{cr}$	Uniaxia	4.39	7.49	11.7
$1.48N_{cr}$	Biaxial	4.42	7.89	12.2
$1.99N_{cr}$	Uniaxia	4.55	11.5	13.9
$1.93N_{cr}$	Biaxial	4.43	7.18	11.4

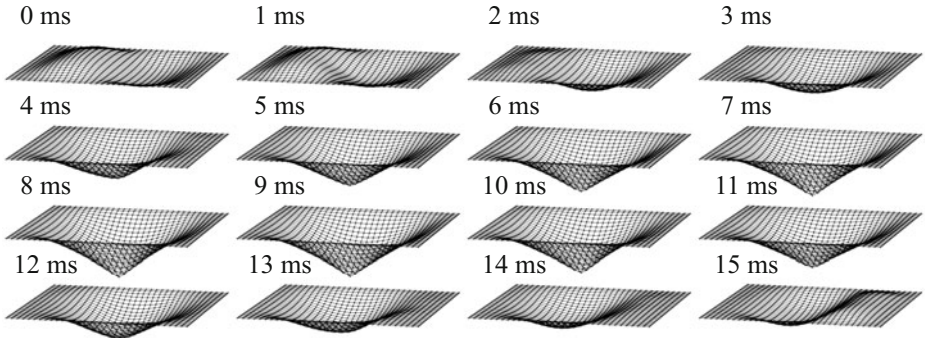

Fig. 16. Deformed shapes of the 400-mm laminate impacted after the second-mode buckling under a uniaxial compressive preload.

critical load is very low. In fact, the critical load must be low enough to be attainable before a first failure is induced, but, at the same time, it must be high enough for the corresponding preload to have a significant influence on the dynamic response. Therefore, it can be concluded that the most dangerous situation may take place in laminates of intermediate span-to-thickness ratio impacted under compression. This danger should be considered with great care by designers, because, in the condition just described, the compressive strength and the instability limit are unfortunately close to each other, which would be desirable for the mechanical properties of the material to be fully exploited.

It is interesting to compare these findings with the experimental results described in [11]. The authors tested laminates of two different span-to-thickness ratios: 100 and 50. In the first case, the observed influence of preload was small, as regards both the impact response parameters (maximum force and contact duration) and the material damage. Even the impact test on the laminate buckled into a two-half-wave shape showed no significant difference with respect to the others. In the second case, where the compressive strength of the undamaged specimen was not much higher than the first critical load, the effect of in-plane loads became important. The highest preload level ($1.2N_{cr}$) led to a strong increase in the delaminated area. The au-

thors conclude that the most detrimental effect of membrane stresses takes place when the critical load is close to the compressive strength and, at the same time, the applied preload is comparable with those two parameters.

The present study provides a satisfactory explanation of these conclusions, showing that the influence of preload strongly depends on the span-to-thickness ratio and that this dependence can be explained by considerations regarding the dynamic behaviour of the target, without the need for a damage model. Obviously, the extent of damage, as well as some complex phenomena reported in [11] (like the instantaneous collapse of the preloaded laminate during impact, observed in one test), do need some modelling of damage, because they possibly involve both the global buckling and the local instability of sublaminates created by delamination, which in turn can affect the propagation of delamination.

5. Conclusions

A number of finite-element analyses were performed in order to evaluate the effect of membrane initial stresses on the low-speed impact behaviour of composite laminates and to study how this effect varies for different span-to-thickness ratios of the target. The results, showing that this ratio actually has a major importance in determining the influence of membrane stresses, can be summarized as follows.

(1) A tensile preload can increase the peak stresses induced by a low-speed impact, thus lowering the impact energy threshold required to initiate damage. These effects are stronger for biaxial than uniaxial preloads, and they become weaker and weaker as the span-to-thickness ratio increases. However, a higher initial speed of impactor leads to a wave-dominated transient behaviour, where these trends are less distinct.

(2) A compressive preload can have beneficial effects on the peak stresses and can increase the impact energy threshold at the lowest span-to-thickness ratios. On the contrary, very slender laminates are practically insensitive to such a preload, even if it is higher than the buckling load. The most detrimental influence of initial stresses was found at medium span-to-thickness ratios, when the compressive strength of the laminate and its buckling load are close to each other, for preloads comparable to the critical load.

A comparison with experimental investigations carried out by other authors indicates that some phenomena and the seeming contradictions among them can be explained by the present results, with considerations regarding the dynamic response of specimens, without taking into account the material degradation due to damage. This is especially true for the effect of preload and different span-to-thickness ratios on the impact energy threshold and on the history of contact force, as well as for the danger represented by compressive preloads in particular conditions. On the other hand, a reliable prediction of the extent of damage, together with a complete understanding of some complex phenomena described in the literature, can be achieved only with a proper modelling of material failure.

REFERENCES

1. S. Abrate, Impact on Composite Structures, Cambridge University Press, Cambridge (1998).
2. C. T. Sun and S. Chattopadhyay, “Dynamic response of anisotropic laminated plates under initial stress to impact of a mass,” J. Appl. Mech. ASME, **42**, No. 3, 693-698 (1975).
3. B. R. Butcher and P. J. Fernback, “Impact resistance of unidirectional CFRP under tensile stress: further experimental variables,” Fibre Sci. Technol., **14**, No. 1, 41-58 (1981).
4. J. K. Chen and C. T. Sun, “Analysis of impact response of buckled composite laminates,” Compos. Struct., **3**, No. 2, 97-118 (1985).
5. C. T. Sun and J. K. Chen, “On the impact of initially stressed composite laminates,” J. Compos. Mater., **19**, No. 6, 490-504 (1985).
6. J. K. Chen and C. T. Sun, “Dynamic large deflection response of composite laminates subjected to impact,” Compos. Struct., **4**, No. 1, 59-73 (1985).

7. B. V. Sankar and C. T. Sun, "Low-velocity impact damage in graphite-epoxy laminates subjected to tensile initial stresses," AIAA J., **24**, No. 3, 470-471 (1986).
8. M. D. Robb, W. S. Arnold, and I. H. Marshall, "The damage tolerance of GRP laminates under biaxial prestress," Compos. Struct., **32**, Nos. 1-4, 141-149 (1995).
9. S. T. Chiu, Y. Y. Liou, Y. C. Chang, and C. I. Ong, "Low velocity impact behavior of prestressed composite laminates," Mater. Chem. Phys., **47**, Nos. 2-3, 268-272 (1997).
10. A. D. Kelkar, J. Sankar, K. Rajeev, R. J. Aschenbrenner, and G. Schoeppner, "Analysis of tensile preloaded composites subjected to low-velocity impact loads," in: 39th AIAA/ASME/ASCE/AHS/ASC Struct., Struct. Dynam. Mater. Conf., Pt. 3, Long Beach (CA, USA), (1998), pp. 1978-1987.
11. X. Zhang, G. A. O. Davies, and D. Hitchings, "Impact damage with compressive preload and post-impact compression of carbon composite plates," Int. J. Impact Eng., **22**, No. 5, 485-509 (1999).
12. B. Whittingham, I. H. Marshall, T. Mitrevski, and R. Jones, "The response of composite structures with pre-stress subject to low velocity impact damage," Compos. Struct., **66**, Nos. 1-4, 685-698 (2004).
13. T. Mitrevski, I. H. Marshall, R. S. Thomson, and R. Jones, "Low-velocity impacts on preloaded GFRP specimens with various impactor shapes," Compos. Struct., **76**, No. 3, 209-217 (2006).
14. S. M. R. Khalili, R. K. Mittal, and N. M. Panah, "Analysis of fiber reinforced composite plates subjected to transverse impact in the presence of initial stresses," Compos. Struct., **77**, No. 2, 263-268 (2007).
15. I. H. Choi, "Low-velocity impact analysis of composite laminates under initial in-plane load," Compos. Struct., **86**, Nos. 1-3, 251-257 (2008).
16. G. Minak and D. Ghelli, "Influence of diameter and boundary conditions on low velocity impact response of CFRP circular laminated plates," Composites, Pt. B: Eng., **39**, No. 6, 962-972 (2008).
17. D. Ghelli, "Dynamic numerical analysis of composite plates and shells with geometrical nonlinearity," in: J. Soric, F. Gruttmann, and W. Wagner (eds.), Proc. Spec. Workshop Adv. Numer. Anal. Shell-Like Struct., Croat. Soc. Mech., Zagreb (HR) (2007), pp. 161-168.
18. T. J. R. Hughes and T. E. Tezduyar, "Finite elements based upon Mindlin plate theory with particular reference to the four-node bilinear isoparametric element," J. Appl. Mech. ASME, **48**, No. 3, 587-596 (1981).
19. K. J. Bathe, "Finite element procedures in engineering analysis," Prentice-Hall, Englewood Cliffs (1982).
20. S. P. Timoshenko and S. Woinowski-Krieger, "Theory of plates and shells," McGraw-Hill, Singapore (1959).
21. P. Underwood, "Dynamic relaxation," in: T. Belytschko and T. J. R. Hughes (eds.), Computational Methods for Transient Analysis, North-Holland, Amsterdam (1983), pp. 245-265.
22. S. H. Yang and C. T. Sun, Indentation Law for Composite Laminates, NASA CR-165460 (1981).
23. S. W. Tsai and E. M. Wu, "A general theory of strength for anisotropic materials," J. Compos. Mater., **5**, No. 1, 58-80 (1971).